THE ASTROPHYSICAL JOURNAL, 531:503–520, 2000 March 1

α CENTAURI AB

D. B. GUENTHER
Department of Astronomy and Physics, Saint Mary's University, Halifax, N.S., Canada, B3H 3C3; guenther@ap.stmarys.ca
AND
P. DEMARQUE
Center for Solar and Space Research, Department of Astronomy, Yale University, New Haven, CT 06520-8101; demarque@astro.yale.edu
Received 1999 June 4; accepted 1999 October 15

ABSTRACT

Detailed models of α Centauri A and B based on the *Hipparcos*, Yale, and Söderhjelm parallaxes are compared. The consequences of the uncertainty in mass, luminosity, surface temperature, and composition on the structure and the *p*-mode pulsation spectrum of the models are presented. All of the models were constructed using the most current stellar structure physics available to us, including helium and heavy-element diffusion, OPAL (Lawrence Livermore Opacity Library) equation of state, and OPAL and Alexander opacities. Self-consistent models of α Cen A and B that satisfy the observational constraints have an initial helium mass fraction $Y_{\rm ZAMS} = \sim 0.28$. The age of the system depends critically on whether or not α Cen A has a convective core. If it does (our best model), then α Cen AB is ∼7.6 Gyr old, and if it does not, then the binary system is ∼6.8 Gyr old. Both ages and $Y_{\rm ZAMS}$ are accurate to $\pm \sim 10\%$ owing to observational uncertainties. The Galactic enrichment parameter ($\Delta Y/\Delta Z$) for our best model pair is less than 1. Pulsation analyses of our best models yield an average large and small spacing of 101 ± 3 μHz and 4.6 ± 0.4 μHz, respectively, for α Cen A, and 173 ± 6 μHz and 15 ± 1 μHz for α Cen B. Some methodologies that use *p*-mode frequency observations to constrain the system further are outlined. We include a simple test to determine whether or not α Cen A has a convective core and introduce a method to use the small frequency spacing to determine the age of system, overcoming the limitation that it is also sensitive to composition.

Subject headings: binaries: visual — stars: fundamental parameters — stars: individual (α Centauri) — stars: interiors — stars: oscillations

1. INTRODUCTION

To date the most stringent tests of the theory of stellar structure and evolution have been carried out for the Sun. We know the Sun's mass, luminosity, and radius to better than 1 part in 10^3; we know its age, 4.53 Gyr, from meteoritic dating, to within 0.04 Gyr; and we know its observable surface chemical composition to better than ±5% (Guenther 1989; Guenther & Demarque 1997). We also now know the run of sound speed throughout most of the interior, via seismological inversions of the *p*-modes, to better than 1% (Guzik 1998). These constraints, especially the *p*-mode frequencies, have enabled solar model builders to test much of the input physics, including element diffusion and convective transport. In the case of nearby stars, observationally derived radii and luminosities are known, even in the best of cases, to an accuracy of 1%–10%. For visual binary systems with well-measured parallaxes, the uncertainty in mass determinations is rarely less than 1% and more typically of the order of 5%–10% (Demarque et al. 1986). And, of course, we have no direct means of determining the ages of stars except through stellar evolutionary modeling of stars in binary systems or in clusters. The constraints are not stringent enough to test the physical assumptions of stellar structure and evolution to a level better than ±10%–25%. Astroseismology has the potential to change this situation dramatically (Guenther 1998). For example, the large spacing, which is derived from *p*-mode oscillation data, can be used to determine the radius of a star, which in turn can be used to test convective transport theory. For a star with a well-determined mass, composition, distance, luminosity, and surface temperature, astroseismology can help us test stellar structure theory. For a star with less well-known observables, astroseismology can provide us with information about the star that cannot be obtained by any other means.

To illustrate the very real sensitivity of the *p*-modes to stellar evolution, in Figure 1 we show the $l = 1$ *p*-mode frequencies for an evolving 1 $M_\odot$ star. As the star evolves, the frequencies collapse, that is, the spacing between adjacent *p*-modes decreases. When the hydrogen core of the model nears exhaustion, at ∼8 Gyr, the spacings (see definition of large spacing $\Delta\nu$ in § 5) of the low *n*-valued *p*-modes become irregular. First the $n = 1$ modes are affected; then as the star ages and the helium core mass increases, the $n = 2$ modes are affected; and so on. The irregular spacing is a consequence of mode bumping (also known as avoided crossings), where the frequencies of *g*-modes, trapped in the growing helium core, increase into the region occupied by the lowest *n*-valued *p*-modes. The *p*-mode frequencies are perturbed ("bumped") by the close proximity of the *g*-mode frequencies (Aizenman et al. 1977).

A primary candidate for astroseismology is α Cen A. Because it is nearby and part of the visual binary system α Cen AB, it has a well-determined mass, surface composition, luminosity, and effective temperature. Furthermore, the mass of α Cen A, ∼1.1 $M_\odot$, and the mass of α Cen B, ∼0.9 $M_\odot$, conveniently bracket the mass of the Sun.

Flannery & Ayres (1978) were the first to produce models specifically for α Cen A and B. They tried to construct models of α Cen A and B assuming a solar composition but could not achieve satisfactory fits to the observations. They were able to fit the observational constraints only for

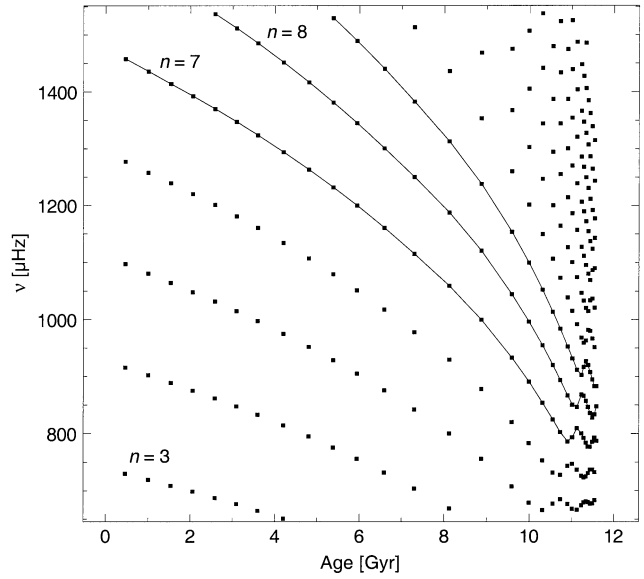

FIG. 1.—Several $l = 1$ p-mode frequencies of an evolving 1 $M_\odot$ star (solar composition) are plotted as a function of age. To aid the eye, lines have been drawn through the $n = 7$, 8, and 9 data points.

models with twice the solar heavy-element abundance. Today, more refined abundance analyses support their conclusion that the α Cen system is more metal-rich than the Sun.

Following the report of Fossat et al. (1984) of a possible detection of p-mode oscillations on α Cen A, Demarque et al. (1986) constructed models of α Cen A to test the p-mode identifications. They found no agreement between their model-predicted frequencies, specifically the large spacing, and the observed frequencies. They also analyzed existing ground-based parallax and orbital measurements (circa 1986) to obtain the masses of the components. Their values, in common use since, must now be revised owing to the new parallax determinations.

Noels et al. (1991) introduced a general procedure for fitting models to the binary system. They kept as free parameters Z, Y, age, and α, which they assumed to be the same for both stars, and used the observed values of effective temperature and luminosity to constrain the system. In order to examine the parameter space, they calculated the first-order partial derivative dependencies of luminosity and effective temperature with respect to the four free parameters from a grid of evolutionary tracks with varying Y, Z, and α.

Edmonds et al. (1992) relaxed the constraint, previously assumed, that the mixing-length parameter, α, is the same for α Cen A and α Cen B. Their models (for α Cen A and B) were also the first to include the effects of helium diffusion. They applied the observed value for Z (a free parameter in Noels et al. 1991) to their models to make up for the removed constraint. To fit their models to observation, they first calibrated Y by fitting the models, with solar α, to the observed luminosity, and then they calibrated α by fitting the models, with the previously calibrated Y, to the observed effective temperature. Unlike the Noels et al. (1991) fitting strategy, their procedure does not provide a completely self-consistent determination of α and Y, in that once α is calibrated, the original Y value needs to be recalibrated for the new α, and the whole procedure iterated until the values converge. They found that the mixing-length parameter for α Cen A is slightly smaller than for α Cen B but did not include an uncertainty analysis to determine if the difference is significant.

Lydon, Fox, & Sofia (1993) tested their formulation of stellar convection on α Cen A and B. They parameterized the convective and radiative energy flux, determined from their three-dimensional simulations of deep, efficient convection (Lydon, Fox, & Sofia 1992), as a function of standard thermodynamic variables. They then replaced the mixing-length approximation and its adjustable parameter α with their parameterless description of convection. They obtained models that approximately fitted α Cen A and B's position in the H-R diagram and thereby were the first to model a star with a description of convection that does not include an adjustable free parameter to determine the radius. Their simulation of convection does not follow the important shallow convection regime where the greatest sensitivity to radius occurs; hence, as expected, their models only roughly match α Cen A and B's H-R diagram positions.

In their careful analysis, Frenandes & Neuforge (1995) also use α Cen A and B to test models of convection, including the Canuto and Mazzitelli formulation (Canuto & Mazzitelli 1991, 1992). Of interest here is their attempt to determine whether or not the two stellar components require unique mixing-length parameters. Owing to the uncertainties in their models (and the uncertainties in the observational constraints), they were unable to determine if the α's are distinct.

Even though α Cen AB is one of the best-observed stellar systems, one finds that the uncertainties in the model-deduced physical characteristics of the stars are too large to test stellar structure theory. This is exemplified by the large variation in published ages for α Cen AB, which range from 4 to 8 Gyr. The broad range in derived characteristics are in part caused by the relatively large uncertainties in some of the observational constraints. The amount of scatter caused by the stellar modeling physics itself is unknown and untested in stars other than the Sun.

How close are we, with regard to existing observational constraints, to being able to test the physics of stellar structure and evolution? How exactly can astroseismology help improve this situation? In this paper we will address these questions. We will describe our renewed effort to produce detailed models of α Cen A and B, constructed with the latest physics, including helium and heavy-element diffusion, and subject to the latest observational constraints, including those derived from the new *Hipparcos* parallax, which is significantly different from the formerly adopted Yale parallax. Additionally, as we anticipate that p-modes will soon be observed[1] on α Cen A (and B), we will investigate the effects of uncertainties in the constraints on the p-mode frequencies. This uncertainty analysis will enable us to identify which features of the p-mode spectrum are best suited to help further constrain the system.

Our study of α Cen AB is partly motivated by the tremendous advances being made in modeling stellar convection and adapting it to actual stellar structure and evolution calculations. We believe that one of the first applications of astroseismology will be to test stellar convection models

[1] Unfortunately, neither the COROT or MOST space missions will be able to observe α Cen AB owing to the inclination of their orbits.

and theory. Nearly all stellar models that have a convective envelope, which includes the solar model and models of α Cen A and B, are based on the mixing-length approximation (hereafter MLA) as formulated by Böhm-Vitense (Vitense 1953; Böhm-Vitense 1958). In the MLA convective energy is assumed to be carried by an element of fluid of fixed size that rises adiabatically a specific distance and then is instantly absorbed by its surroundings through radiative diffusion. In stellar structure the mixing-length distance, the distance the fluid element rises, is assumed to be proportional to the pressure scale height; the constant of proportionality is called the mixing-length parameter α, which is an adjustable parameter of the MLA. The MLA predicts that the temperature gradient in most of the stellar convective envelope is very slightly superadiabatic. Near the surface of the star, where convective transport efficiency drops and radiative transport efficiency rises, there is a peak in the temperature gradient that climbs well above the adiabatic temperature gradient. This region, which is only 0.04% $R_\odot$ thick in the Sun, called the superadiabatic layer (SAL), establishes the radii of stars that have convective envelopes.

Although stellar astrophysicists are well aware of the limitations of the MLA, it is only recently that both numerical models of convection and seismological probes of the Sun's convective envelope have been used to test the theory in the stellar astrophysical regime. Indeed, numerical convection models show that for deep convection (efficient convection), the temperature gradient is very nearly adiabatic (Chan & Sofia 1987, 1989), as predicted by the MLA. But for shallow convection, more appropriate for describing the SAL, numerical convection models show that the SAL is not accurately described by the MLA (Stein & Nordlund 1989; Dravins & Nordlund 1990; Kim 1993; Kim et al. 1995, 1996a, 1996b; Nordlund & Stein 1996). Furthermore, the frequencies of high-l p-modes calculated from solar models based on the MLA do not match the observed frequencies whereas models that are based on three-dimensional convection simulations do (Demarque et al. 1999)

Because the SAL is very near the surface, high-l p-modes, which are currently undetectable in stars, are needed to fully resolve the structure of the SAL. The low-l p-modes, though, can discern gross features of the SAL and are enough, for example, to show that the MLA is not adequate for the Sun. And even though astroseismology may not be able to provide enough information to predict the structure of the SAL in stars, the observable low-l p-modes do constrain the gross features of the outer layers, and they do fix the radius.[2]

[2] The depth of the convective envelope, and hence the radius of the star, is determined by the specific entropy S (Schwarzschild 1958) of the convection zone, which is given by

$$S = \int dS = C_p \int_{P_{\rm base}}^{P_{\rm surface}} (\nabla - \nabla_{\rm ad}) d\ln P \, ,$$

where C_p is the specific heat at constant pressure P, ∇ is the temperature gradient, $\nabla_{\rm ad}$ is the adiabatic temperature gradient, $P_{\rm base}$ is the pressure at the base of the convective envelope, and $P_{\rm surface}$ is the pressure at the surface. The integrand is effectively zero throughout all of the convection zone except in the thin SAL, where the contribution to the integral is the largest. Because the width, height, and shape of the superadiabatic peak depends on the opacity, equation of state, surface boundary condition (set by the atmosphere model), and the mixing-length parameter α, the depth of the convective envelope itself, as set by the specific entropy, also depends on these quantities.

Another concern stellar theorists have with the MLA has to do with the universality of the mixing-length parameter itself: Does the solar-tuned value give correct radii when applied to other stars? Although a "universal value" of the mixing-length parameter is usually adopted when calculating stellar models, tracks, and isochrones for a specific population of stars, there is no physical justification for this. Because the MLA enables us to calculate stellar radii, which determine a star's position in the H-R diagram, the value of α and its variation, as a function of mass, within a stellar cluster affect our determination of the cluster's age.

Most work to date on stellar convection has been focused on the Sun. Because we anticipate p-mode data to become available for other stars, we hope that soon we will be able to test the applicability of the MLA and the new three-dimensional models of convection on these stars. Ground-based networks of telescopes, with instruments specifically designed to see p-mode oscillation frequencies in the Doppler shifts of spectral lines, such as the AFOE (Advanced Fiber Optic Echelle; Brown et al. 1991), are being tested on several nearby bright stars. In addition, two space-platformed telescopes designed to observe small luminosity variations in stars, *MOST* (Microvariability and Oscillations of Stars) and *COROT* (Convection and Rotation; Baglin & Auvergne 1997), are scheduled to be launched by the year 2002. Most recently, Buzasi et al. (2000) have reported seeing radial p-modes on α UMa using the *WIRE* satellite. Their mode frequencies do appear to match theoretical predictions (Guenther et al. 2000). Other microsatellites, not as far along the funding process, are also being developed to observe p-mode oscillations.

In the next section we describe the observational data used to constrain our models of α Cen A and B, and in § 3 we describe the basic physical assumptions of our stellar evolutionary models. In § 4 we describe the results of our model calculations. In § 5 we discuss the p-mode spectra and how they can be used to constrain the system. Finally, in § 6 we summarize our results and conclusions.

2. OBSERVATIONAL CONSTRAINTS

2.1. *Many Parallaxes*

Owing to the high luminosity and large separation of the stellar components of α Cen AB, it is technically difficult to determine accurately the parallax and the orbital elements. In addition, according to Pourbaix et al. (1999), the orbit is slightly irregular, possibly because of an unseen component. In this work we consider three distinct parallaxes for α Cen AB: the parallax obtained from *Hipparcos*, 742.12 ± 1.40 mas; our heretofore reference parallax from Demarque et al. 1986 , 750.6 ± 4.6 mas, which was based on the Yale Parallax Catalog value, 749.9 ± 5.4 mas, but derived from a slightly different weighting given to the individual observations; and the recently published value by Söderhjelm (1999) that combines *Hipparcos* and ground-based observations, 747.1 ± 1.2 mas. A fourth parallax, which we are not considering in this work, has recently been published by Pourbaix et al. (1999), 737.0 ± 2.6 mas, that is lower still than the *Hipparcos* parallax. We must reserve judgment on this parallax until further results can confirm or dismiss this result. We do note the models that Pourbaix et al. constructed for α Cen A and B, based on their parallax determination, are widely separated in age, 2.7 Gyr and 6.2 Gyr, respectively; hence, they are unlikely to be realistic models

of α Cen A and B.

2.2. *Masses*

We continue to use the orbital data from Heintz (1982) for the separation $a = 17''.515 \pm 0''.015$ and the period $P = 79.920$ yr. And we continue to use the mass ratio of Kamper & Wesselink (1978) $f = 0.454 \pm 0.002$, a result recently confirmed by Pourbaix et al. (1999). The masses derived from these orbital elements and the *Hipparcos*, Yale, and Söderhjelm parallaxes are listed in Table 1. The lower parallax of Pourbaix et al. (1999) gives significantly higher masses, $M_\odot = 1.16 \pm 0.031\ M_\odot$ and $M_B = 0.97 \pm 0.032\ M_\odot$.

2.3. *Effective Temperature*

For estimates of $T_{\rm eff}$ we rely on the recent summary of published values provided in Table 1 of Neuforge-Verhechke & Magain (1997). Effective temperature determinations for α Cen A range from a low of 5710 K to a high of 5830 K. The high value, we note, is the determination of Neuforge-Verhechke and Magain based on high-resolution and high signal-to-noise ratio spectra. We adopt $T_{\rm eff,A} = 5770 \pm 50$ K. The surface temperature determinations for α Cen B also vary over a range of approximately 100 K, from 5250 to 5350 K. We adopt a value $T_{\rm eff,B} = 5300 \pm 50$ K.

2.4. *Metallicity*

The values of [Fe/H] obtained from spectroscopic-based analyses, of course, depend on the assumed values of surface temperature. We ignore this dependency and simply adopt an extensive range in Z to account for all likely possibilities. From Table 1 in Neuforge-Verhechke & Magain (1997) we note that published values of $[{\rm Fe/H}]_{\rm A}$ range from -0.01 to $+0.28$ and values of $[{\rm Fe/H}]_{\rm B}$ range from -0.05 to $+0.38$. Because our models of α Cen A and B, as we will show, depend critically on Z, we have chosen initially to analyze a wide range of possible values for Z from solar to twice solar, i.e., from $Z = 0.02$ to $Z = 0.04$ for both α Cen A and α Cen B. Later, when we want to constrain a unique pair of models for pulsation and uncertainty analysis, we will adopt values near those reported by Chmielewski et al. (1992), $[{\rm Fe/H}]_{\rm A} = 0.22 \pm 0.02$ and $[{\rm Fe/H}]_{\rm B} = 0.26 \pm 0.02$. These values, we note, are consistent with the adopted $T_{\rm eff}$. With $(Z/X)_\odot = 0.0245$ (Grevesse et al. 1996) this gives $(Z/X)_{\rm A} = 0.041 \pm 0.002$ and $(Z/X)_{\rm B} = 0.045 \pm 0.002$. Although we assume the initial (zero-age main-sequence) values of X and Y, i.e., $X_{\rm ZAMS}$ and $Z_{\rm ZAMS}$, are identical for both stars, helium and heavy-element diffusion, which we include in our models, well affect the surface abundance of X and Z for α Cen A and α Cen B differently; hence, we do expect [Fe/H] to be different for α Cen A and B.

2.5. *Luminosities*

The luminosities we derive here are based on the visual magnitudes published in the *Hipparcos* catalog, which are within 0.02 mag of those published in the 4th edition of the Yale Bright Star Catalog (see Table 1). The bolometric corrections were obtained by linearly interpolating the color-correction tables of Green et al. (1987) in $T_{\rm eff}$, [Fe/H], and

TABLE 1

α CEN A B CONSTRAINTS

Name	Value	Source
Parallax π (arcsec)	0.7506 ± 0.0046	Yale (Demarque et al. 1986)
	0.74212 ± 0.0014	*Hipparcos* Catalog
	0.7471 ± 0.0012	Soderhjelm 1999
Separation a (arcsec).....	17.515 ± 0.002	Heintz 1982
Period P [yr].....	79.920	Heintz 1982
Mass ratio f	0.454 ± 0.002	Kamper&Wesselink 1978
$M_{\rm bol}$ (s)	4.79	Revised Yale Isochrones
$V_{\rm A}$	-0.01 ± 0.01	*Hipparcos* Catalog
$V_{\rm B}$	1.35 ± 0.01	*Hipparcos* Catalog
$(B-V)_{\rm A}$	0.71 ± 0.04	*Hipparcos* Catalog
$(B-V)_{\rm B}$	0.90 ± 0.02	*Hipparcos* Catalog
$({\rm BC})_{\rm A}$	-0.059 ± 0.041	Revised Yale Isochrones
$({\rm BC})_{\rm B}$	-0.194 ± 0.021	Revised Yale Isochrones
$M_{\rm A}\ [M_\odot]$	1.0844 ± 0.008	Based on Yale Parallax
	1.1238 ± 0.008	Based on *Hipparcos* Parallax
	1.1015 ± 0.008	Based Soderhjelm Parallax
$M_{\rm B}\ [M_\odot]$	0.9017 ± 0.007	Based on Yale Parallax
	0.9344 ± 0.007	Based on *Hipparcos* Parallax
	0.9159 ± 0.007	Based on Soderhjelm Parallax
$\log (L_{\rm A}/L_\odot)$	0.1924 ± 0.017	Based on Yale Parallax
	0.2027 ± 0.017	Based on *Hipparcos* Parallax
	0.1969 ± 0.017	Based on Soderhjelm Parallax
$\log (L_{\rm B}/L_\odot)$	-0.2977 ± 0.011	Based on Yale Parallax
	-0.2874 ± 0.011	Based on *Hipparcos* Parallax
	-0.2932 ± 0.011	Based on *Hipparcos* Parallax
$T_{\rm eff,A}$	5770 ± 50 K	Neuforge-Verhechke & Magain 1997
$T_{\rm eff,B}$	5300 ± 50 K	Neuforge-Verhechke & Magain 1997
$[{\rm Fe/H}]_{\rm A}$	0.22 ± 0.02	Chmielewski et al. 1992
$[{\rm Fe/H}]_{\rm B}$	0.26 ± 0.02	Chmielewski et al. 1992
$(Z/X)_{\rm A}$	0.041 ± 0.002	Derived (see text)
$(Z/X)_{\rm B}$	0.045 ± 0.002	Derived (see text)

$B-V$. Here we assumed [Fe/H] = 0.25 for both α Cen A and B, we adopted the *Hipparcos* values for $(B-V)_A = 0.71 \pm 0.04$ and $(B-V)_B = 0.90 \pm 0.02$, and took $T_{eff,A} = 5770$ K and $T_{eff,B} = 5300$ K. We obtained $(BC)_A = -0.059$ and $(BC)_B = -0.194$. Our final derived luminosities are listed for each of the three parallaxes in Table 1.

The luminosities derived here are different from Demarque et al. (1986), where we used $\log (L_A/L_\odot) = 0.17$ and $\log (L_B/L_\odot) = -0.32$, but are very close to the recent and commonly adopted values of Noels et al. (1991), $\log (L_A/L_\odot) = 0.1853 \pm 0.015$ and $\log (L_B/L_\odot) = -0.3065 \pm 0.015$. The new *Hipparcos* parallax compared to the Yale parallax accounts for a +0.01 increase in the log of the luminosity.

It is difficult to determine the overall uncertainty in the luminosity. The uncertainty in the bolometric correction (BC), which is dominated by the uncertainty in $B-V$, contributes ±0.016 for α Cen A and ±0.008 for α Cen B to the uncertainty in the log-luminosity derivation. The uncertainty in V estimated to be ±0.01 accounts for ±0.004 uncertainty in the log-luminosity derivation. And finally, the uncertainty in the parallax, which we assume is ±5 mas (to encompass the range of parallaxes we are considering), contributes ±0.005 to the uncertainty in the log-luminosity. Assuming the contributing uncertainties are independent, the total uncertainty *by only these factors* in $\log (L_A/L_\odot)$ is ±0.017 and $\log (L_B/L_\odot)$ is ±0.011, with the error dominated by the uncertainty in the BC.

3. STELLAR MODELING

3.1. *Model Physics*

We have attempted to carry out as complete and up-to-date an evolutionary analysis of α Cen AB as is reasonably possible. To that aim we have utilized the latest generation of physics, now demanded by solar seismology, in our evolutionary calculations of α Cen A and α Cen B.

All the models were calculated using the Yale stellar evolution code (YREC; Guenther et al. 1992). The initial or zero-age main-sequence (ZAMS) models for α Cen A and B were obtained from pre–main-sequence evolutionary calculations to the ZAMS for stars with the appropriate mass and near-solar composition. Post-ZAMS evolutionary sequences for models with different compositions were obtained by first rescaling the composition of these ZAMS models.

We used the current equation-of-state tables from Lawrence Livermore (Rogers 1986; Rogers, Swenson, & Iglesias 1996). For the interior opacities we used the Lawrence Livermore (OPAL98; Iglesias and Rogers 1996) tables and for the surface and atmosphere opacities we used the tables of Alexander and Ferguson (1994). Both sets of tables are provided in a form that enables interpolation in not only X and Y, but also Z. The stellar evolution code, therefore, can and does use opacities appropriate for the composition of each shell in the model, even when Z varies from shell to shell as it does when heavy-element diffusion is accounted for. The equation of state is not as sensitive to changes in Z as are the opacities. For the equation-of-state tables the code uses a single Z composition table, Z_{ZAMS}, throughout the model.

Because α Cen A and α Cen B are nearly solar-type stars, we choose to use the Krishna-Swamy (1966) atmosphere model rather than the more customary Eddington gray atmosphere. The Krishna-Swamy atmosphere provides an analytical T-τ relation that fits the observed T-τ relation for the Sun out to the temperature minimum in the solar corona. Our choice of atmosphere model perturbs the interior-structure variables by less than one part in 10^4 and, hence, does not greatly affect our conclusions about the age and the composition of α Cen A and B (Guenther et al. 1992). It does, though, affect the p-mode frequencies, which are sensitive to the structure of the outermost layers.

The other basic physics of YREC are described in Guenther et al. (1992) and will not be further described here. For reference, in Table 2 we show the physical characteristics of a solar model constructed with the above described assumptions. Note that this solar model fits the low- and intermediate-l p-mode frequencies ($0 = l = 100$) to better than 3 parts in 10^4.

3.2. *Constraining the Models: An Overview*

In terms of stellar modeling the binary system is defined by 14 parameters, seven for α Cen A: L_A, luminosity; $T_{eff,A}$, effective temperature; M_A, mass; $Y_{ZAMS,A}$, initial helium mass fraction; $Z_{ZAMS,A}$, initial metal mass fraction; A_A, age; and α_A, mixing-length parameter, and a similar set of seven parameters for α Cen B. The binary nature of the system provides three constraints: $Y_{ZAMS,A} = Y_{ZAMS,B}$, $Z_{ZAMS,A} = Z_{ZAMS,B}$, and $A_A = A_B$. In standard stellar evolution Y_{ZAMS}, Z_{ZAMS}, M, A, and α are input, and L and T_{eff} are output. Therefore, modeling α Cen A and α Cen B provides four additional constraints $L_A = L_A(Y_{ZAMS,A}, Z_{ZAMS,A}, A_A, M_A, \alpha_A)$, $T_{eff,A} = T_{eff,A}(Y_{ZAMS,A}, Z_{ZAMS,A}, A_A, M_A, \alpha_A)$, $L_B = L_B(Y_{ZAMS,B}, Z_{ZAMS,B}, A_B, M_B, \alpha_B)$, and $T_{eff,B} = T_{eff,B}(Y_{ZAMS,B}, Z_{ZAMS,B}, A_B, M_B, \alpha_B)$. We need an additional seven constraints to close the system. Six of these are normally taken as the observed values for effective temperature, mass, and luminosity.

We have 13 of the 14 constraints needed to uniquely specify the α Cen AB system. We have chosen not to close the system, as have others in the past, by assuming that the mixing lengths are identical for α Cen A and B. We no longer prefer this assumption because one of the goals of our research, and possibly one of the first applications of astroseismology, is to determine whether or not a single mixing-length parameter is applicable to all stars regardless

TABLE 2

REFERENCE SOLAR MODEL CHARACTERISTICS

Characteristic	Value
X_{ZAMS}	0.70623
Y_{ZAMS}	0.27377
Z_{ZAMS}	0.02000
X_{surf}	0.73798
Y_{surf}	0.24400
Z_{surf}	0.01802
Age	4.55 Gyr
M_{ce}	0.0242 $M_\odot$
R_{ce}	0.7129 $R_\odot$
$\log T_{eff}$	3.7619
M_{bol}	4.79
$\log P_c$	17.374
$\log T_c$	7.1975
$\log \rho_c$	2.1886
α	2.087

of mass, composition, and age. We take as our final constraint Z_{surf}.

We calculated an array of models in Y_{ZAMS} and Z_{ZAMS} for α Cen A and an array of models in Y_{ZAMS} and Z_{ZAMS} for α Cen B. We forced the models to fit the observed T_{eff} and log $(L/L_\odot)$ by adjusting the mixing-length parameter of each of the models. The two arrays of models, one for α Cen A and one for α Cen B, were then compared and models with common Y_{ZAMS} and Z_{ZAMS} as well as age were identified. This yielded a one-dimensional sequence of model pairs (α Cen A and α Cen B). We choose Z_{ZAMS} as the parameter of this sequence, although we could just as easily have chosen age or Y_{ZAMS}. To obtain a unique pair of models, we applied the last constraint to the system, i.e., we selected the model pairs that have the observed Z_{surf}.

3.3. *Some Modeling Details*

To produce a model of α Cen A (the procedure is similar for α Cen B) that matches the observed $T_{eff,A}$ and log $(L_A/L_\odot)$ for a given composition (X_{ZAMS}, Z_{ZAMS}), we rescale the composition in our ZAMS model, and then evolve the model. If the evolutionary track does not pass within ± 0.001 in log $(L_A/L_\odot)$ and ± 0.001 in log $T_{eff,A}$, we adjust the mixing-length parameter α, which for a given luminosity, controls the radius of the model (assuming the model has a convective envelope). Then the track is recalculated. The process is iterated until the track passes within the above noted tolerances of α Cen A's position in the H-R diagram. The entire iterative process is automated in YREC, and thus, YREC produces a fitted model that establishes α, age, Y_{surf}, and Z_{surf} as a function of X_{ZAMS}, Z_{ZAMS}, $T_{eff,A}$ and log $(L_A/L_\odot)$. Two two-dimensional grids ($Y_{ZAMS} \times Z_{ZAMS}$), one for α Cen A and one for α Cen B, were constructed using this process, with Y_{ZAMS} ranging from 0.23 to 0.30 in increments of 0.01 and Z_{ZAMS} ranging form 0.020 to 0.040 in increments of 0.002.

We then plotted age versus Z_{ZAMS} for each Y_{ZAMS} in the array of models. Since the age increases monotonically with increasing Z_{ZAMS} and since the rate of increase is different for α Cen A and B, the age versus Z_{ZAMS} curves for α Cen A cross the curves for α Cen B. At the points of intersection, if they exist, α Cen A and α Cen B have identical age, Y_{ZAMS}, and Z_{ZAMS}. Because the points of intersection are obtained by simple linear interpolation, and because the physical characteristics of a stellar model, in particular its age, are not linear functions of, for example, Y_{ZAMS} and Z_{ZAMS}, the intersection data are only approximate.

Finally, we plotted the surface $(Z/X)_A$ and $(Z/X)_B$ as a function of Z_{ZAMS} and applied the Z_{surf} constraint to obtain a unique pair of models for the α Cen AB system. The final pair of models were used in our pulsation and uncertainty analysis.

4. α CEN A AND α CEN B MODELS

As outlined in the preceding section, we began by constructing a grid of models spanning a range in Y_{ZAMS} and Z_{ZAMS} for both α Cen A and B. Even though the models have distinct compositions, all were tuned, via adjustments to the mixing-length parameter, to have the observed luminosity and effective temperature. The top two panels of Figure 2 show the evolutionary tracks of several of the α Cen A models. The location of α Cen A in the H-R diagram is identified by the single data point with error bars. The specific (Y_{ZAMS}, Z_{ZAMS}) compositions are identified in the figure. The tracks are diverse, owing in part to the existence or nonexistence of a convective core (see lower two panels in Fig. 2). If a convective core develops during the evolution of the model, fresh hydrogen is mixed into the core that

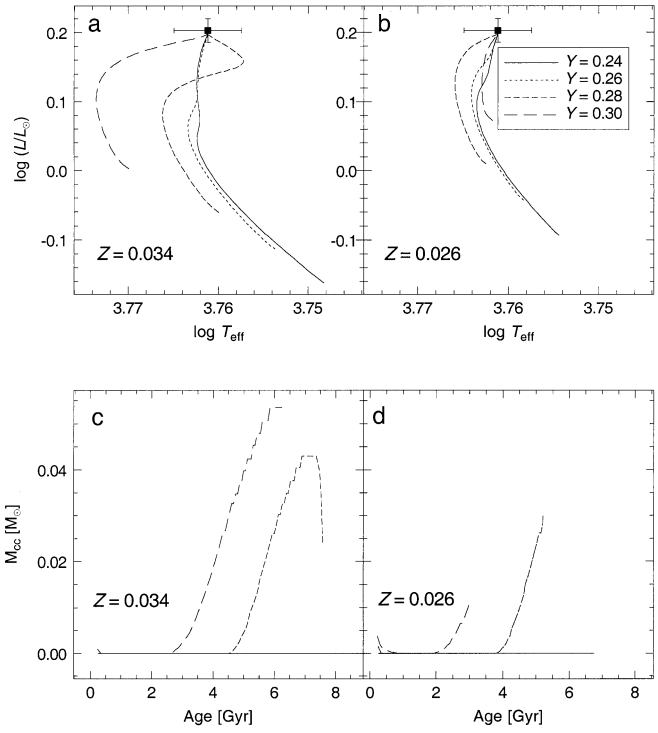

FIG. 2.—Panels (*a*) and (*b*) show evolutionary tracks for a selected group of models of α Cen A. The position of α Cen A in the H-R diagram is indicated by the square data point with error bars. The models in panel (*a*) have $Z_{ZAMS} = 0.034$ and the models in panel (*b*) have $Z_{ZAMS} = 0.026$. Plots of the time evolution of the mass of the convective core, M_{cc}, corresponding to the models plotted in panels (*a*) and (*b*) are shown below in panels (*c*) and (*d*), respectively.

extends the star's main-sequence lifetime. If not, core hydrogen exhaustion occurs earlier, and so does the star's evolutionary journey toward the giant branch. The lower two panels in Figure 2 plot M_{cc}, the mass of the convective core in solar masses, versus age for the corresponding tracks in the panels above. The models whose tracks are *C* shaped correspond to models that have convective cores. These models still have some hydrogen fuel left in their cores, $X_c > 0.01$, whereas the models that do not develop convective cores are nearly exhausted of hydrogen in their cores with $X_c < 0.0001$.

The convective cores develop shortly after the ignition of CNO burning. Because the nuclear luminosity of CNO burning depends on the temperature to a high power (~ 15), it dumps heat into the core at a much greater rate than into the cooler surrounding regions, and as a consequence convection starts. CNO burning will begin when the temperatures and densities in the core are high enough. Increasing Y both increases the core density and the central temperatures; hence, models of α Cen A with greater Y are more likely to develop convective cores from CNO burning than models with lower Y.

Having produced hundreds of models of α Cen A and B, all with distinct Y_{ZAMS} and Z_{ZAMS}, we next need to apply the constraint of common age and ZAMS composition to the models. This was accomplished graphically via plots similar to those shown in Figure 3. In Figure 3, each panel shows a plot of the age versus Z_{ZAMS} for a given Y_{ZAMS}. All of the models calculated for α Cen A and B are represented. Models based on the *Hipparcos*, Yale, and Söderhjelm parallaxes, which fix the mass and luminosity of the models, are shown, distinguished by the different line styles.

From each plot we located the point of intersection, *for a specific parallax*, of the α Cen A and α Cen B curves. This *intersection point*, subject to the uncertainties of linear interpolation, corresponds to a pair of models for the α Cen AB system that have common age, Y_{ZAMS}, and Z_{ZAMS}. The combined set of intersection points from each plot forms a linear sequence of α Cen AB model pairs as a function of Y_{ZAMS}. The sequence could be equally as well characterized by Z_{ZAMS} or age. We chose to characterize the sequence by Z_{ZAMS} because it is closely tied to the final constraint Z_{surf}.

We caution that the α Cen A curves for each parallax, plotted in Figure 3, should only be matched with the α Cen B curves of the same parallax. The intersection of one parallax curve with a different one does not define, for example, an error region associated with the parallaxes. This is because the published uncertainties for each parallax mea-

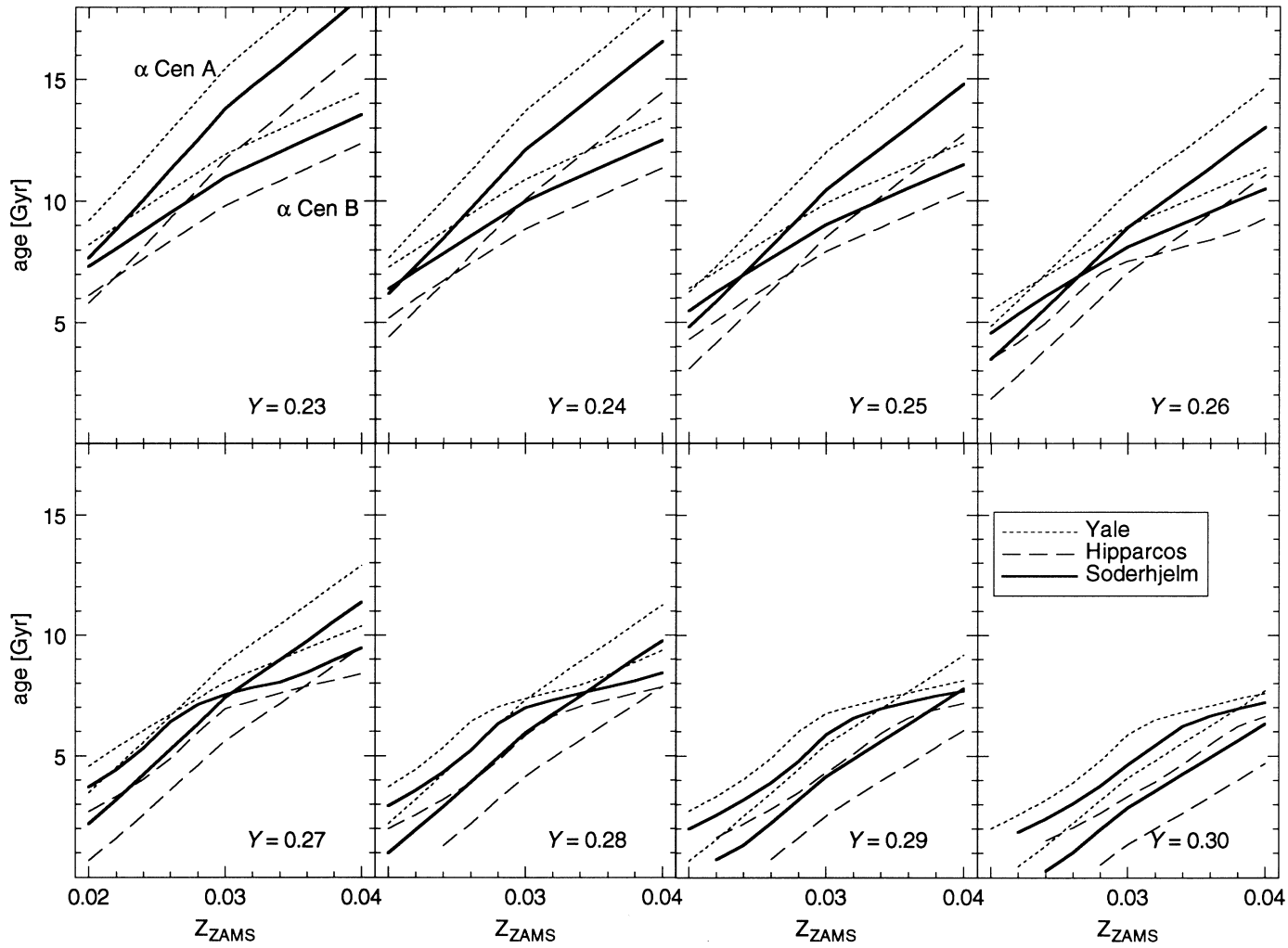

FIG. 3.—Plots of age versus Z_{ZAMS} for models of α Cen A and α Cen B are shown. Each panel contains models for a specific Y_{ZAMS}. Three different sets of models were constructed, one each for the Yale, *Hipparcos*, and Söderhjelm parallaxes. For a given parallax, the points of intersection of the lines in each panel corresponds to a pair of models (α Cen A and α Cen B) that have common age, Z_{ZAMS}, and Y_{ZAMS}.

surement are smaller than the spread of parallaxes considered and because it is improbable that the parallax of α Cen A is different from the parallax of α Cen B, which is what one would be assuming if one measures the intersection points from two distinct parallax curves.

The uncertainties associated with the parallax are represented in Figure 4, which plots age versus Z_{ZAMS} for just the intersection points. There is a jump that occurs in the common age of α Cen A and B between $Z_{ZAMS} = \sim 0.027$ and $Z_{ZAMS} = 030$. This marks the transition from models of α Cen A that do not develop a convective core during their evolution, to the left, to models that do, to the right. Convection in the core extends the main-sequence lifetime of α Cen A models, which, as a consequence, raises the age of the intersection points. Figure 4 shows that even accepting the broader uncertainty defined by the spread in published parallaxes, rather than the tighter uncertainties quoted for each individual parallax, the age of the system is confined to a small 1 Gyr range centered on 7.2 Gyr. It appears that the age uncertainty could be refined still further given a precise Z_{ZAMS} value, but, as we discuss next, the uncertainties in Y_{surf}, Z_{surf}, T_{eff}, mass, and luminosity ultimately prevent a more precise determination of the age.

To estimate the effect of uncertainties in mass, luminosity, effective temperature, helium abundance, and metallicity on the models, we selected the pair of models that lie on the curve for the Söderhjelm parallax in Figure 4 and that have $(Z/X)_{surf}$ closest to the observed values (see Table 1). The physical characteristics of these models are listed in the first row of Tables 3 and 4, for α Cen A and B, respectively. The initial composition values for these models are: $Y_{ZAMS} = 0.280$ and $Z_{ZAMS} = 0.034$. With these models as reference, we calculated new models perturbing individually the L, M, T_{eff}, Y_{ZAMS}, and Z_{ZAMS}. The magnitude of the perturbation is listed in the second column. The L perturbation is in units of log $L/L_\odot$, the M perturbation is in units of $M_\odot$, the T_{eff} perturbation is in units of K. For example, the model identified as "A-ΔL" in Table 3 is similar to the reference model A, except that it was constrained, during the evolutionary modeling, to have a final log-luminosity 0.01 less than the reference model. Below the first line of data in Tables 3 and 4, corresponding to the perturbed models, the columns list the magnitude of the effect that the perturbations have on X_{surf}, Z_{surf}, Age (in Gyr), α, M_{cc}, M_{env} (mass of the convective envelope in units of $M_\odot$), x_{env} (radius fraction location of the base of the convective envelope), log P_c (log central pressure in dyne cm^{-2}), log T_c (log central temperature in K), log ρ_c (log central density in g cm^{-3}), $\langle \Delta\nu \rangle$ (averaged large p-mode spacing in μHz), $\langle \delta\nu_0 \rangle$ (averaged $l = 0$ small spacing in μHz), and $\langle \delta\nu_1 \rangle$ (averaged $l = 1$ small spacing in μHz).

With respect to the age, uncertainties in the composition (models A $\pm$ ΔY, A $\pm$ ΔZ in Table 3 and models B $\pm$ ΔY, B $\pm$ ΔZ in Table 4) appear to have the biggest effect. Indeed, the combined rms error in age for α Cen B from Z_{ZAMS} and Y_{ZAMS} is more than ± 2 Gyr, 4 times the age scale shown in Figure 4! This may explain the great variation in published ages for α Cen AB. From our vantage point, and as we discuss in the next section, we believe that astroseismology has the potential to reduce the volume of the error space.

In Figure 5 we plot α for α Cen A and B, obtained by linear interpolation, opposite Z_{ZAMS}. For each parallax, α Cen A and B maintain distinct values of α for all Z_{ZAMS}. Referring to Tables 3 and 4, we see, though, that the effect of uncertainties in T_{eff}, Y_{ZAMS}, and Z_{ZAMS} ($\sim \pm 0.2$ for α Cen A and $\sim \pm 0.3$ for α Cen B) are so large that it is not possible to state definitively whether or not α Cen A and B do indeed have distinct mixing-length parameters.

In Figure 6 we plot Z_{ZAMS} versus Y_{ZAMS}, where Y_{ZAMS} for the intersection points was obtained by linear interpolation. The relationship is nearly linear: $Y_{ZAMS} = 2.657 \times Z_{ZAMS} + 0.187$.

The connection between Z_{ZAMS} and the observed metallicity for α Cen A and B is shown in Figure 7, which plots

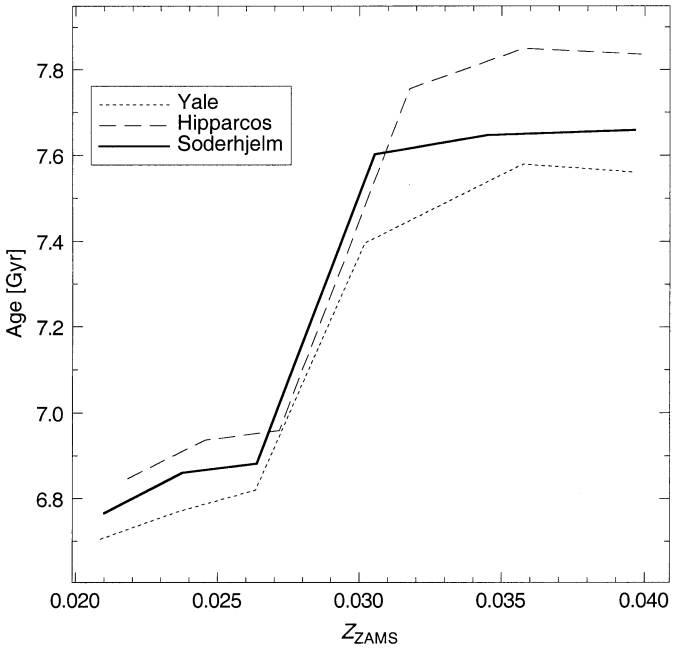

FIG. 4.—Age versus Z_{ZAMS} is shown for the (interpolated) models at the points of intersection identified in Fig. 3.

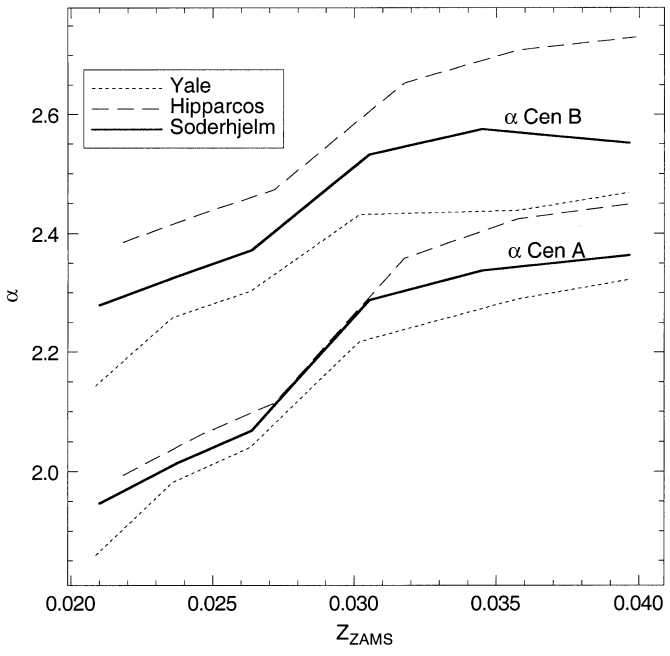

FIG. 5.—Mixing-length parameter α versus Z_{ZAMS} is shown for the (interpolated) models at the points of intersection identified in Fig. 3.

TABLE 3

α CEN A UNCERTAINTIES

Model	Perturbation	X_{surf}	Z_{surf}	Age	α	M_{cc}	M_{env}	x_{env}	log P_c	log T_c	log ρ_c	X_c	Z_c	$\langle\Delta\nu\rangle$	$\langle\delta\nu_0\rangle$	$\langle\delta\nu_1\rangle$
A		0.7277	0.03023	7.583	2.33	0.0241	0.0415	0.6674	17.6195	7.3393	2.4763	0.011	0.037	101.20	4.62	7.26
A−ΔL ...	−0.010	−0.0010	0.0001	−0.108	0.05	0.0107	0.0055	−0.0069	−0.0533	−0.0043	−0.0521	0.008	0.000	1.60	−0.27	−0.02
A+ΔL ...	0.010	−0.0001	0.0000	−0.044	−0.06	−0.0014	−0.0014	0.0008	0.0179	0.0039	0.0170	−0.002	0.000	−1.70	0.06	−0.12
A−ΔM...	−0.008	0.0004	−0.0001	0.118	−0.03	−0.0059	−0.0008	−0.0009	0.0308	0.0010	0.0329	−0.003	0.000	−0.37	0.10	−0.08
A+ΔM...	0.008	−0.0015	0.0002	−0.258	0.03	0.0147	0.0052	−0.0056	−0.0630	−0.0032	−0.0637	0.009	0.000	0.23	−0.42	−0.11
A−ΔT ...	−50.000	0.0007	−0.0001	−0.051	−0.16	0.0036	−0.0019	0.0021	−0.0112	0.0010	−0.0111	0.001	0.000	−2.56	0.00	−0.09
A+ΔT ...	50.000	−0.0017	0.0002	−0.085	0.16	0.0070	0.0059	−0.0074	−0.0273	0.0004	−0.0277	0.003	0.000	2.48	−0.26	−0.09
A−ΔY ...	−0.010	0.0106	−0.0003	0.461	0.01	−0.0241	−0.0013	−0.0003	0.1088	−0.0304	0.1408	−0.006	0.000	0.11	0.19	−0.10
A+ΔY ...	0.010	−0.0114	0.0003	−0.638	−0.01	0.0216	0.0049	−0.0055	−0.0971	−0.0077	−0.0981	0.017	0.000	−0.19	−0.36	−0.02
A−ΔZ ...	−0.004	0.0043	−0.0036	−0.591	−0.06	0.0128	−0.0022	0.0052	−0.0797	−0.0126	−0.0814	0.022	−0.005	−0.10	−0.02	0.44
A+ΔZ ...	0.004	−0.0040	0.0036	0.521	0.07	−0.0219	0.0033	−0.0084	0.1131	−0.0133	0.1293	−0.007	0.005	0.05	0.22	−0.43

TABLE 4

α CEN B UNCERTAINTIES

Model	Perturbation	X_{surf}	Z_{surf}	Age	α	M_{cc}	M_{env}	x_{env}	log P_c	log T_c	log ρ_c	X_c	Z_c	$\langle\Delta\nu\rangle$	$\langle\delta\nu_0\rangle$	$\langle\delta\nu_1\rangle$
B.....		0.7178	0.03067	7.443	2.54	0.0000	0.0651	0.6605	17.2792	7.1540	2.1322	0.347	0.037	173.00	15.04	25.48
B−ΔL ...	−0.010	−0.0031	0.0003	−0.813	−0.05	0.0000	0.0006	0.0015	−0.0238	−0.0067	−0.0311	0.034	0.000	3.06	0.76	1.21
B+ΔL ...	0.010	0.0012	−0.0001	0.193	−0.13	0.0000	−0.0014	−0.0011	0.0103	0.0042	0.0134	−0.014	0.000	−3.06	−0.44	−0.72
B−ΔM...	−0.008	0.0020	−0.0002	0.614	−0.03	0.0000	0.0008	−0.0030	0.0154	0.0042	0.0231	−0.023	0.000	−0.87	−0.42	−0.68
B+ΔM...	0.008	−0.0040	0.0004	−1.214	−0.16	0.0000	−0.0019	0.0042	−0.0296	−0.0068	−0.0416	0.045	0.000	0.79	0.74	1.17
B−ΔT ...	−50.000	0.0006	−0.0001	−0.081	−0.33	0.0000	−0.0040	0.0014	−0.0015	−0.0001	−0.0012	0.002	0.000	−5.04	−0.41	−0.66
B+ΔT ...	50.000	−0.0024	0.0003	−0.539	0.18	0.0000	0.0033	−0.0010	−0.0126	−0.0026	−0.0172	0.019	0.000	5.07	0.72	1.16
B−ΔY ...	−0.010	0.0130	−0.0004	1.523	0.23	0.0000	0.0064	−0.0084	0.0260	0.0057	0.0388	−0.040	0.001	−0.02	−0.74	−1.19
B+ΔY ...	0.010	−0.0150	0.0006	−1.858	−0.32	0.0000	−0.0066	0.0087	−0.0343	−0.0071	−0.0508	0.057	−0.001	−0.02	0.96	1.54
B−ΔZ ...	−0.004	−0.0006	−0.0032	−1.493	−0.25	0.0000	−0.0075	0.0098	−0.0254	−0.0101	−0.0407	0.058	−0.005	−0.07	0.87	1.38
B+ΔZ ...	0.004	0.0004	0.0031	1.572	0.29	0.0000	0.0086	−0.0108	0.0286	0.0112	0.0436	−0.056	0.005	0.06	−0.90	−1.40

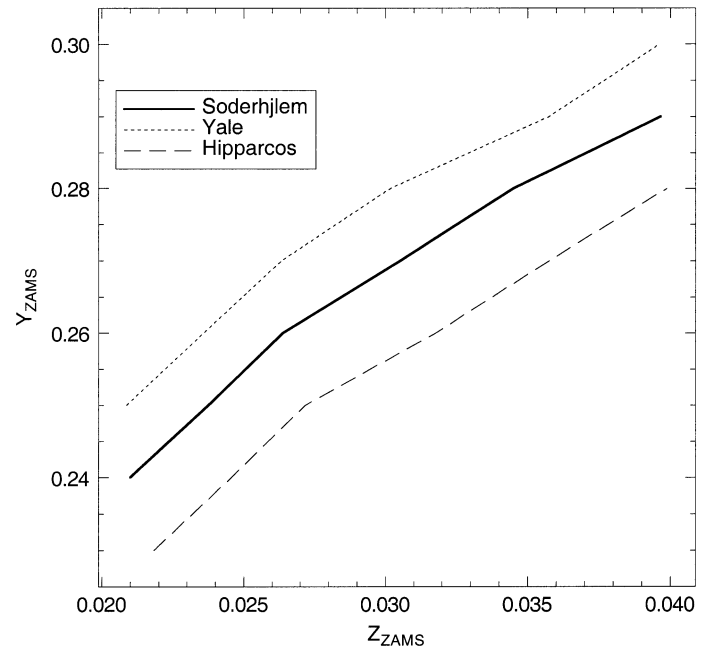

FIG. 6.—Y_{ZAMS} versus Z_{ZAMS} is shown for the (interpolated) models at the points of intersection identified in Fig. 3.

$(Z/X)_{surf}$ for α Cen A and B as a function of Z_{ZAMS}. The observed $(Z/X)_{surf}$ values and error range (also shown in Fig. 7) were derived from the [Fe/H] values of Chmielewski et al. (1992) calibrated to the solar abundances of Grevesse et al. (1995). Ignoring observational uncertainties for the moment, our models, which do include both helium and heavy-element diffusion, demonstrate that α Cen B retains more of its primordial metals at the surface than α Cen A. Within the observational uncertainties though, this difference is not distinguishable. Our reference models, A and B, lie within the error bars of the observed surface metallicities for α Cen A and B.

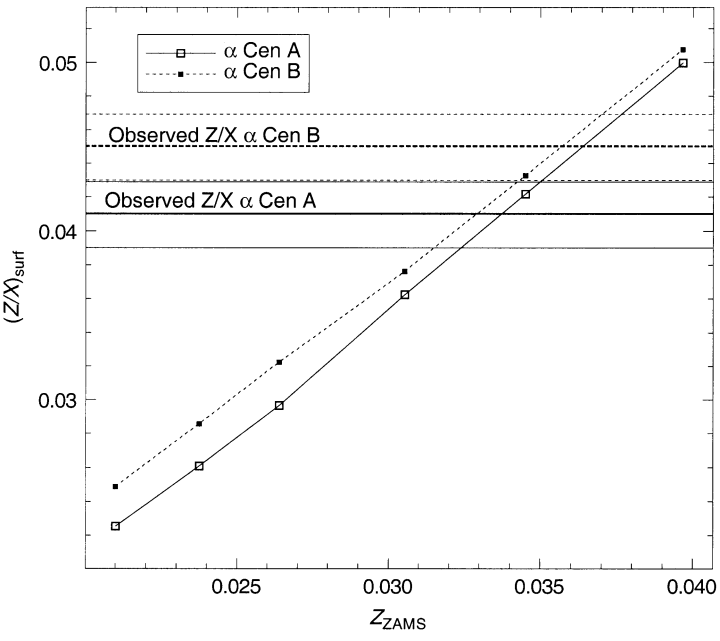

FIG. 7.—Surface metal to hydrogen mass fraction ratio $(Z/X)_{surf}$ vs. Z_{ZAMS} is shown for the intersection-point models of α Cen A and α Cen B identified in Fig. 3. The observed values and error bar range of $(Z/X)_{surf}$ for α Cen A and α Cen B (Chmielewski et al. 1992) are indicated by the horizontal lines.

In summary, we have presented a viable methodology for determining the structural and evolutionary state of α Cen A and B. Unfortunately, the uncertainties in current observational constraints prevents us from narrowing in on a small range of possible models. The uncertainties in composition and T_{eff} are particularly troublesome with regard to pinning down the age and mixing-length parameters. Although the age of our reference models A and B is 7.6 Gyr, the observational uncertainties expand the uncertainty of this determination to ±2 Gyr. And, although we do derive distinct mixing-length parameters for models of α Cen A and B, again, the effect of observational uncertainties prevents us for conclusively stating whether or not this difference is significant.

We have conservatively assumed that the observational uncertainties are themselves independent and that the uncertainties associated with α Cen A are independent of those associated with α Cen B, except in the case of the parallaxes. This is not completely valid and a relaxation of this assumption would probably reduce the error space, possibly by up to a factor of 2.

5. PULSATION ANALYSIS

Low-l p-mode frequencies were calculated for all of the models in Tables 3 and 4 using Guenther's stellar pulsation code (Guenther 1994). The calculation of p-mode frequencies includes nonadiabatic corrections for radiation in the Eddington approximation. The numerical accuracy of the calculation is better than ±0.1 μHz for models with ~2000 shells, as are our models of α Cen A and B. We estimate that the uncertainties associated with the pulsation physics, based on studies of models of the Sun, are less than approximately ±0.3 μHz at low frequencies, increasing to approximately ±3 μHz at higher frequencies, where unaccounted for nonadiabatic effects due to convection-oscillation interactions take place (Guenther & Demarque 1997). Indeed, it is believed that the solar p-modes are driven by turbulence near the SAL, and presumably a similar driving mechanism exists in the near solar-like α Cen A and B.

The large spacings, $\Delta\nu \equiv \nu(n, l) - \nu(n-1, l)$, and the small spacings, $\delta\nu_l \equiv \nu(n, l) - \nu(n-1, l+2)$, for the models listed in Tables 3 and 4 were calculated. Here, n is the radial order, l is the azimuthal order, and ν is the frequency. Averages of the large and small spacings were also calculated. For the large spacing, the average $\langle\Delta\nu\rangle$ was obtained over $n = 14$–24 and $l = 0$–3 for α Cen A, corresponding to the frequency range ~1500 μHz to ~2500 μHz, and over $n = 7$–13 and $l = 0$–3 for α Cen B, also corresponding to the frequency range ~1500 μHz to ~2500 μHz. For the small spacings, the average $\langle\delta\nu_0\rangle$ was obtained over $n = 14$–24 and $l = 0$ for α Cen A, and over $n = 7$–13 and $l = 0$ for α Cen B. The average $\langle\delta\nu_1\rangle$ is similar to $\langle\delta\nu_0\rangle$ except that $l = 1$ modes were selected. The averaged spacings are listed in Tables 3 and 4. From these tables we estimate the large spacing $\langle\Delta\nu\rangle_A = 101 \pm 3$ μHz for α Cen A, and $\langle\Delta\nu\rangle_B = 173 \pm 6$ μHz for α Cen B.

Figure 8 shows the large spacing plotted as a function of frequency for all of the models in Tables 3 and 4. In each panel along the top row, the reference A model is plotted with a solid line, and the perturbed models, as indicated in

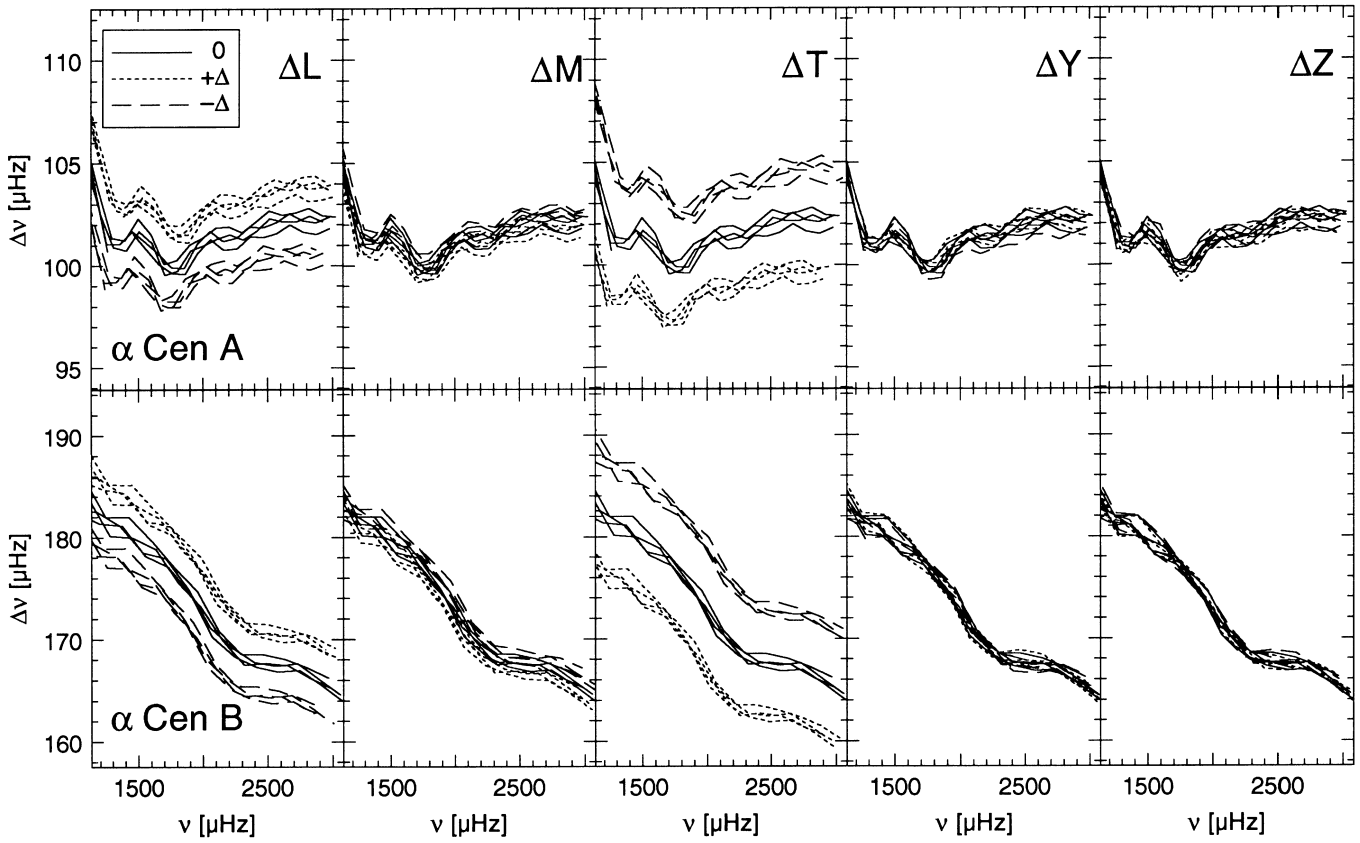

FIG. 8.—Large spacings $\Delta\nu$ versus frequency ν are shown for the $l = 0$, 1, 2 and 3 p-modes. The top row of panels show plots for α Cen A. The p-mode spacings for the reference model A in Table 3 are indicated by solid lines. The p-mode spacings for the perturbed models, e.g., A + ΔL and A − ΔL, are indicated by dashed lines, with the ΔL panel displaying the A $\pm$ ΔL (and reference model) p-mode spacings, and the ΔM, ΔT, ΔY, and ΔZ panels showing p-mode spacings for the A $\pm$ ΔM, A $\pm$ ΔT, A $\pm$ ΔY, and A $\pm$ ΔZ perturbed models. The bottom row of panels are similar to the top row except that they correspond to models for α Cen B.

the legend, are plotted with dashed lines. Along the bottom row, the reference B model is plotted with a solid line.

The large spacing is well known, from asymptotic theory, to be primarily sensitive to the stellar radius. Therefore, it comes as no surprise that perturbations to the luminosity and $T_{\rm eff}(L \propto R^2 T_{\rm eff}^4)$ produce the greatest effect on $\Delta\nu$. Furthermore, the ΔY and ΔZ panels show that changes to $Y_{\rm ZAMS}$ and $Z_{\rm ZAMS}$ have little affect on $\Delta\nu$.

When the p-mode spectrum is first observed on α Cen A (similarly for α Cen B), the large spacing will probably be the first characteristic of the spectrum identified (Guenther 1998)—seen as a peak in the Fourier transform of the power spectrum. The large spacing provides a very precise means of determining the radius of the star, uncontaminated to any significant degree by uncertainties in the star's composition.

The small spacing, also revealed as a peak in the Fourier transform of the power spectrum, is sensitive to the structure of the core, specifically the derivative of the sound speed. Figure 9 shows the small spacings plotted as a function of frequency for all of the models in Tables 3 and 4, using the same key as in Figure 8. Because so many factors can alter the density stratification in the core, it is not too surprising that all the perturbations affect the small spacings to some extent. The largest effects are produced by changes to $Y_{\rm ZAMS}$ and $Z_{\rm ZAMS}$. Curiously, for α Cen A, changes to $Y_{\rm ZAMS}$ mostly affect the $l = 0$ small spacing, and changes to $Z_{\rm ZAMS}$ mostly affect the $l = 1$ small spacings.

Historically, it was initially believed that the small spacing could be used to constrain the age of a star, but later it was realized that this is true only if the composition is known (Ulrich 1986). As we see from Figure 9, the small spacing is too sensitive to other uncertainties, in particular, the composition, to serve exclusively as an age constraint. Minimally the small spacing can be used to reduce the volume of the total error space, as noted by Brown et al. (1991). But we believe there is a way to use the small spacings of both stars in a binary system to determine the age of the system. The method, which uses the fact that the two stars have a common age and composition, is outlined in the summary and conclusions section.

The small spacing can be useful in constraining the model, if it is applied to a star in a particular phase of evolution. For α Cen A, all of the models in Table 3 have convective cores. We see, as shown in Figure 10, which plots $\langle \delta\nu_0 \rangle$ opposite $M_{\rm cc}$ for all the α Cen A models in Table 3, that the small spacing is proportional, with negative slope, to the mass in the convective core. In fact, this relationship is maintained for *all* the perturbed models. Therefore, if α Cen A is near the evolutionary phase that our models indicate, $\langle \delta\nu_0 \rangle$ can be used to determine the mass of the convective core.

There is another feature of the p-mode spectrum of α Cen A that can be used to constrain the system. It is the uneven large spacing at low-l and low-n (for nonradial modes only) caused by mode mixing or mode bumping. As a star

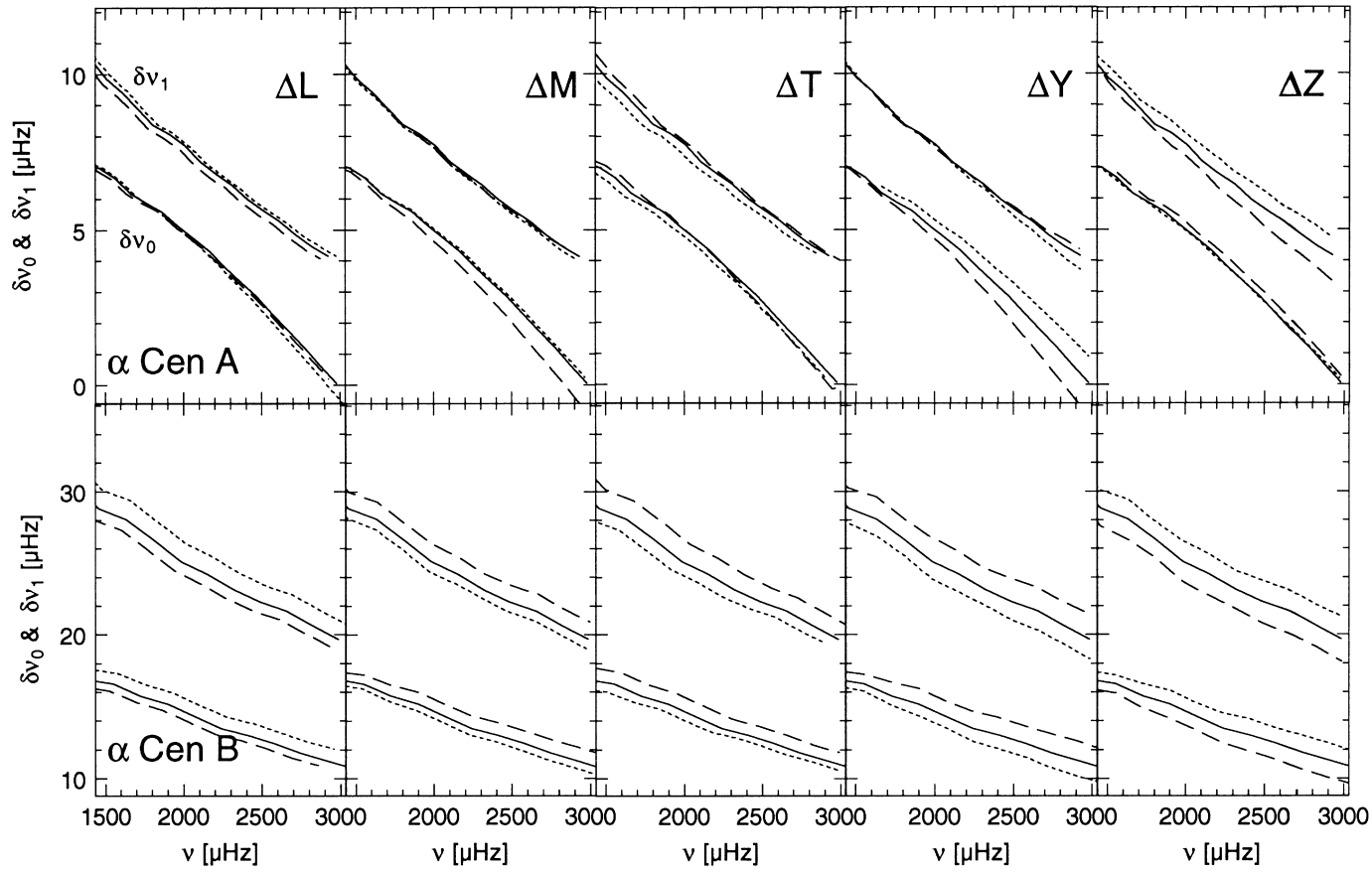

FIG. 9.—Small spacings $\delta\nu_0$ and $\delta\nu_1$ vs. frequency ν are shown. The top row of panels shows plots for α Cen A and the bottom row of panels shows plots for α Cen B. The *p*-mode spacings for the reference model and the perturbed models are as described in Fig. 8.

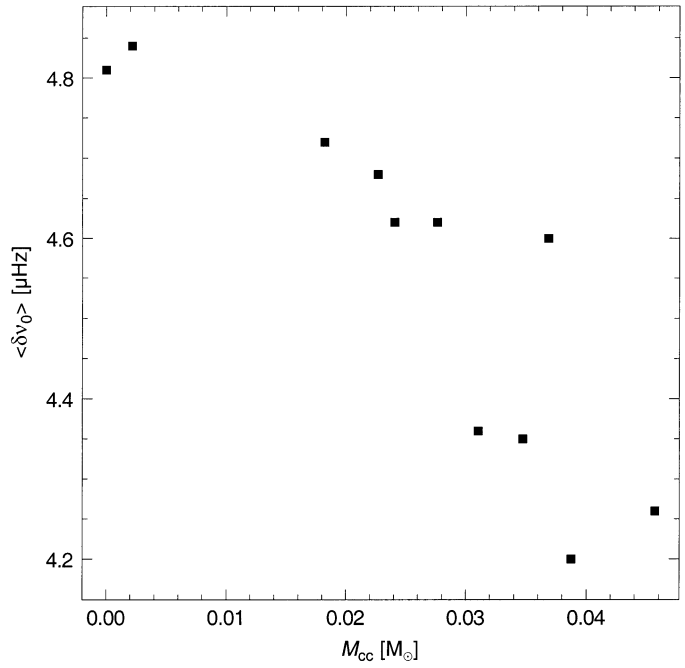

FIG. 10.—Averaged small spacings $\langle\delta\nu_0\rangle$ (see text for definition) are shown plotted as a function of convective core mass for the reference and perturbed models (see Table 3) for α Cen A.

evolves, its core density increases, and as a consequence the frequencies of its *g*-mode spectrum increase bumping into the *p*-mode spectrum (Guenther 1991). For a specific evolved stellar model, one sees, as a consequence of mode bumping, *p*-modes that have dual or mixed mode character. That is, the eigenfunction of the *p*-mode exhibits the phase characteristics of a *g*-mode near the core, and a *p*-mode throughout the rest of the star. The *g*-mode/*p*-mode mix perturbs the frequencies of the affected *p*-mode. In Figure 11, similar to Figure 8, we plot the large spacings as a function of frequency for lower frequencies. In this frequency range, some of the $l = 1, 2$, and 3 *p*-modes are mixed (see Tables 5 and 6), and as a consequence, their frequencies are perturbed. As shown the large spacing, which defines the frequency separation between adjacent *p*-modes, can be significantly perturbed. The effect of the model perturbations on the location of the mode-bumped spacings (i.e., the downward spikes in Fig. 11) is unique for each perturbation. As expected, $T_{\rm eff}$, which does not directly affect the core, has no effect on the mode bumping. Mode bumping, on the other hand, is extremely sensitive to composition.

How can the mode bumpings be used to constrain the models, assuming one can actually observe individual *p*-modes at low frequencies? We can imagine several applications. We believe mode bumping can be used to help identify the individual modes in the *p*-mode spectrum.

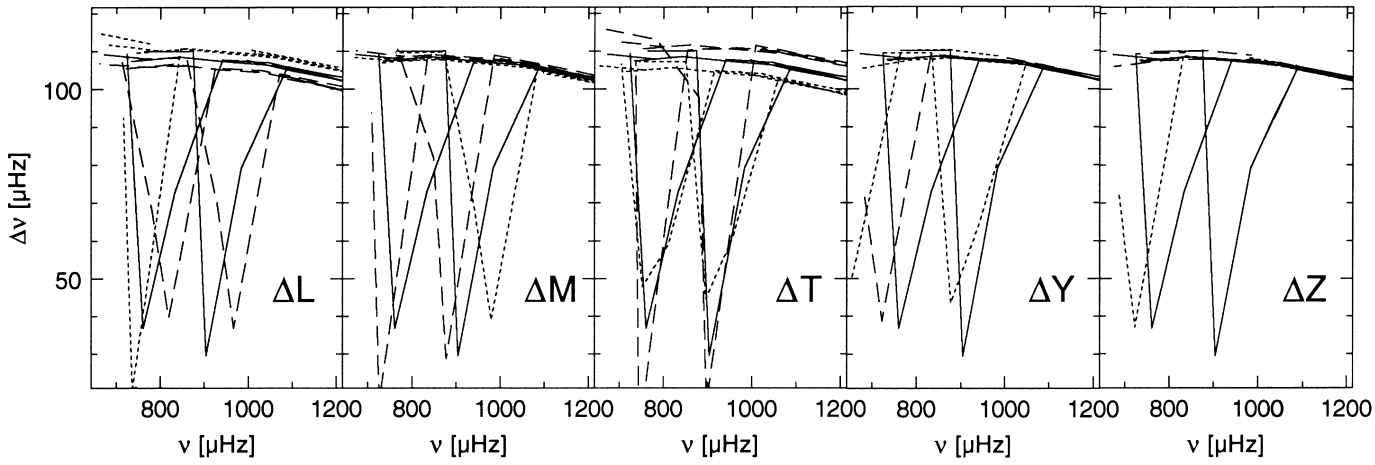

FIG. 11.—Large spacings v versus frequency v are shown for the $l = 0, 1, 2$, and 3 p-modes for the reference and perturbed models of α Cen A (see Table 3). These plots are similar to those shown along the top row of Fig. 8, except that a lower frequency range is shown, where mode bumping (see text) occurs.

Observers have no means of identifying the azimuthal and radial order of p-modes on stars except by comparisons to model predictions. But because the modes are regularly spaced, with one frequency range looking almost the same as another, it is extremely difficult to "zero" the n and l order of the spectrum (for the Sun we can spatially resolve the modes across the disk, which makes the mode identifications, by comparison, easy). The spectrum in the region of the mode bumping is not regularly spaced, and therefore, we believe it can be used to identify the lowest order p-modes, from which the rest of the spectrum can be fixed. The mode-bumped spacings can be used to determine the phase of evolution of the star. As noted in the discussion of Figure 1, the upper limit of the n-value of the affected p-modes increases with increasing stellar age, hence, by noting at which n-value the irregularly spaced p-modes begin one can then determine the age of the model, via diagrams similar to Figure 1. Another application, which is less clear to us at this stage, is the possibility of "inverting" the p-mode frequencies in this region to constrain the core regions.

For reference purposes we include Tables 5 and 6, which list the individual frequencies for model A, in Table 5, and model B, in Table 6. The table lists, from left to right, l the azimuthal order, n the radial order, n_p the component of the radial order that is p-mode in character, n_g the component of the radial order that is g-mode in character, $\nu_{\rm ad}$ the adiabatic frequency, $\nu_{\rm R:nonad}$ the real component of the nonadiabatic frequency, $\nu_{\rm I:nonad}$ the imaginary component of the nonadiabatic frequency, $\Delta\nu$, and $\delta\nu$.

In summary, we have outlined how we imagine the p-mode frequencies can be used to help constrain our models of α Cen A and B. Specifically, we note that the large spacing, being relatively insensitive to everything but the radius, will be useful in constraining the radius of α Cen A and B. The situation for the small spacing is more cumbersome. Regardless, we point out that for models of α Cen A the $l = 0$ small spacing could be useful in constraining the mass of the convective core. Finally, we point out that if our models of α Cen A are correct, then the lowest frequency p-modes exhibit mode bumping. We suggest that the irregular frequency spacing between adjacent p-modes caused by the mode bumping will be useful in fixing the absolute identification of the radial and azimuthal order of the p-modes, where no other method currently exists, and can be used to determine the age of the system. At this stage, we are necessarily vague about how these mode bumpings can be used to constrain the structure of the core, to which they are indeed very sensitive.

6. SUMMARY AND CONCLUSIONS

We have produced a reference model for α Cen A and B and have estimated the effect of observational uncertainties on the physical characteristics of the models. In addition, we have discussed the potential usefulness of future p-mode observations to further constrain the models.

Our models indicate that α Cen AB is approximately 6–8 Gyr old. Currently observational uncertainties, primarily in composition, limit the accuracy of our age determination. Although the quoted error for [Fe/H] is ± 0.02, the published values of [Fe/H] encompass a much larger range with a scatter of ± 0.1. If we adopt the value and error bar of Chmielewski et al. (1992; see Tables 1 and 3) then the age of α Cen A is well determined at 7.6 ± 0.8 Gyr, where we have also included the contributions to the uncertainty from Y. But if we more conservatively accept the larger scatter of published [Fe/H] values as representative of the typical uncertainty in [Fe/H], then the age determination becomes bimodal because of the presence or absence of a convective core in models of α Cen A. If α Cen A does not have a convective core, corresponding to $Z_{\rm ZAMS} < \sim 0.03$, then α Cen AB is 6.8 ± 0.8 Gyr old. We suspect that the wide range of ages associated with previously published models of α Cen A and B are a consequence of the uncertainties in composition. The total contribution to the age uncertainty from uncertainties in the parallax and the BC's are much smaller by comparison.

We find that the mixing-length parameter, α, in our α Cen A models is $\sim 10\%$ smaller than α in our α Cen B models, but we also find that the effect of the composition and surface temperature uncertainties on α is greater than this difference. Therefore, we are unable to state whether or not α Cen A and B have similar mixing-length parameters. The uncertainties in composition and $T_{\rm eff}$ need to be reduced by a factor of four to begin to allow us to test convection theory.

Because the large p-mode frequency spacing is primarily sensitive to the radius of a star and insensitive to composi-

TABLE 5

α CEN A (MODEL A) $P-$MODE DATA

l	n	n_p	n_g	$\nu_{\rm ad}$	$\Delta\nu_{\rm R:nonad}$	$\nu_{\rm I:nonad}$	ν	$\delta\nu$
0.....	4	4	0	626.3	626.3	0.00		
0.....	5	5	0	733.8	733.8	0.00	107.5	
0.....	6	6	0	842.4	842.4	0.00	108.6	
0.....	7	7	0	949.7	949.7	0.00	107.3	
0.....	8	8	0	1056.0	1056.0	0.01	106.3	
0.....	9	9	0	1159.7	1159.7	0.01	103.7	
0.....	10	10	0	1260.5	1260.4	0.03	100.7	
0.....	12	11	0	1361.2	1361.2	0.07		
0.....	13	12	0	1462.8	1462.7	0.14	101.5	7.00
0.....	14	13	0	1563.7	1563.6	0.25	100.8	6.68
0.....	15	14	0	1663.9	1663.6	0.43	100.1	6.18
0.....	16	15	0	1763.7	1763.3	0.68	99.6	5.88
0.....	17	16	0	1863.4	1862.9	0.95	99.6	5.59
0.....	18	17	0	1964.3	1963.5	1.30	100.6	5.15
0.....	19	18	0	2065.9	2064.8	1.74	101.3	4.75
0.....	20	19	0	2167.1	2165.6	2.25	100.8	4.33
0.....	21	20	0	2268.4	2266.4	2.85	100.8	3.81
0.....	22	21	0	2370.4	2367.9	3.48	101.4	3.33
0.....	23	22	0	2472.3	2469.3	4.15	101.4	2.86
0.....	24	23	0	2574.6	2570.9	4.96	101.6	2.30
0.....	25	24	0	2677.5	2672.9	5.90	102.0	1.75
0.....	26	25	0	2780.1	2774.5	6.94	101.7	1.21
0.....	27	26	0	2882.8	2876.0	8.20	101.5	0.63
0.....	28	27	0	2985.9	2977.9	9.66	101.8	0.06
1.....	3	4	1	563.5	563.5	0.00		
1.....	4	5	1	672.7	672.7	0.00	109.2	18.81
1.....	5	6	1	780.6	780.6	0.00	107.9	16.73
1.....	7	8	1	889.0	889.0	0.00		
1.....	8	8	0	996.6	996.6	0.00	107.6	13.85
1.....	9	9	0	1101.4	1101.4	0.01	104.8	12.57
1.....	10	10	0	1203.9	1203.9	0.02	102.5	11.44
1.....	11	11	0	1304.9	1304.8	0.05	100.9	10.99
1.....	12	12	0	1405.6	1405.6	0.09	100.7	10.49
1.....	13	13	0	1507.4	1507.3	0.18	101.7	9.86
1.....	14	14	0	1608.6	1608.4	0.32	101.1	9.43
1.....	15	15	0	1708.2	1708.0	0.53	99.6	8.90
1.....	16	16	0	1808.2	1807.7	0.80	99.8	8.37
1.....	17	17	0	1909.1	1908.5	1.10	100.8	8.10
1.....	18	18	0	2010.4	2009.5	1.48	101.0	7.72
1.....	19	19	0	2112.1	2110.8	1.97	101.3	7.18
1.....	20	20	0	2214.0	2212.3	2.53	101.5	6.80
1.....	21	21	0	2315.8	2313.6	3.13	101.3	6.45
1.....	22	22	0	2418.1	2415.3	3.80	101.7	5.98
1.....	23	23	0	2521.0	2517.6	4.55	102.3	5.61
1.....	24	24	0	2623.9	2619.7	5.39	102.1	5.27
1.....	25	25	0	2727.0	2721.9	6.42	102.2	4.84
1.....	26	26	0	2830.5	2824.3	7.58	102.4	4.47
1.....	27	27	0	2933.9	2926.5	8.90	102.1	4.16
2.....	3	4	1	613.8	613.8	0.00		
2.....	4	5	1	723.1	723.1	0.00	109.3	
2.....	5	5	0	759.9	759.9	0.00	36.8	
2.....	6	6	0	833.0	833.0	0.00	73.1	
2.....	7	7	0	940.8	940.8	0.00	107.8	
2.....	8	8	0	1047.8	1047.8	0.00	107.0	
2.....	9	9	0	1151.9	1151.9	0.01	104.1	
2.....	10	10	0	1253.0	1253.0	0.03	101.1	
2.....	11	11	0	1354.1	1354.0	0.07	101.1	
2.....	12	12	0	1455.8	1455.7	0.13	101.7	
2.....	13	13	0	1557.0	1556.9	0.24	101.2	
2.....	14	14	0	1657.7	1657.5	0.42	100.6	
2.....	15	15	0	1757.8	1757.4	0.66	99.9	
2.....	16	16	0	1857.8	1857.3	0.93	99.9	
2.....	17	17	0	1959.2	1958.4	1.28	101.1	

TABLE 5—*Continued*

l	n	n_p	n_g	ν_{ad}	$\nu_{R:nonad}$	$\nu_{I:nonad}$	$\Delta\nu$	$\delta\nu$
2.....	18	18	0	2061.2	2060.1	1.71	101.7	
2.....	19	19	0	2162.8	2161.3	2.22	101.2	
2.....	20	20	0	2264.6	2262.6	2.82	101.4	
2.....	21	21	0	2367.1	2364.6	3.44	101.9	
2.....	22	22	0	2469.5	2466.4	4.12	101.9	
2.....	23	23	0	2572.4	2568.6	4.94	102.1	
2.....	24	24	0	2675.8	2671.1	5.87	102.5	
2.....	25	25	0	2779.0	2773.3	6.92	102.2	
2.....	26	26	0	2882.2	2875.4	8.18	102.1	
2.....	27	27	0	2985.9	2977.8	9.65	102.4	
3.....	3	4	1	653.9	653.9	0.00		
3.....	4	5	1	763.9	763.9	0.00	110.0	
3.....	5	6	1	874.1	874.1	0.00	110.1	
3.....	6	6	0	903.5	903.5	0.00	29.5	
3.....	7	7	0	982.8	982.8	0.00	79.3	
3.....	8	8	0	1088.8	1088.8	0.01	106.1	
3.....	9	9	0	1192.5	1192.5	0.02	103.7	
3.....	10	10	0	1293.9	1293.8	0.04	101.4	
3.....	11	11	0	1395.1	1395.1	0.09	101.2	
3.....	12	12	0	1497.5	1497.4	0.17	102.3	
3.....	13	13	0	1599.1	1599.0	0.30	101.6	
3.....	14	14	0	1699.3	1699.1	0.51	100.1	
3.....	15	15	0	1799.8	1799.3	0.77	100.3	
3.....	16	16	0	1901.0	1900.4	1.06	101.0	
3.....	17	17	0	2002.7	2001.7	1.43	101.4	
3.....	18	18	0	2104.9	2103.6	1.92	101.9	
3.....	19	19	0	2207.2	2205.5	2.46	101.9	
3.....	20	20	0	2309.4	2307.1	3.06	101.6	
3.....	21	21	0	2412.1	2409.3	3.72	102.2	
3.....	22	22	0	2515.4	2512.0	4.45	102.7	
3.....	23	23	0	2618.7	2614.5	5.29	102.5	
3.....	24	24	0	2722.2	2717.1	6.31	102.6	
3.....	25	25	0	2826.1	2819.9	7.45	102.8	
3.....	26	26	0	2929.8	2922.3	8.75	102.5	
3.....	27	27	0	3033.6	3024.7	10.39	102.4	

tion, it and a well-established parallax could provide the necessary factor of four improvement in the T_{eff} determinations. Since [Fe/H] determinations depend sensitively on the assumed values of T_{eff}, with better atmosphere models that include a more realistic treatment of convection (which affects the line profiles), one should in principle be able to reduce the uncertainties in the observed composition. We therefore see no obstacles, once *p*-modes are observed, in carrying out tests of stellar convection on α Cen A and B.

We find that α Cen A is in a unique evolutionary phase where a small perturbation to the composition of the model determines whether or not the model has a convective core. As noted above, the presence of a convective core affects the age determination—a convective core lengthens the main-sequence (core hydrogen burning phase) lifetime and, as a consequence, increases the derived age of α Cen AB by ~ 1 Gyr.

We examined three unique parallax determinations: the Yale parallax, upon which nearly all models of α Cen A and B have been based; the *Hipparcos* parallax; and, halfway between them, the recently published Söderhjelm parallax, which blends together ground and *Hipparcos* observations. Our reference models are based on the Söderhjelm parallax. We are able to produce self-consistent models of α Cen A and α Cen B that match the observed metallicity and have $Y_{ZAMS} = 0.28$. This composition is consistent with the expectations of Galactic nucleosynthesis modeling. We cannot rule out the Yale and *Hipparcos* parallaxes because observational uncertainties in other parameters, such as composition, dominate the uncertainties in our calculations. A fourth parallax (Pourbaix et al. 1999) was brought to our attention as we were writing up the results of this work that is different enough from the parallaxes we have considered—it is 5 mas smaller than the *Hipparcos* parallax and 10 mas smaller than the Söderhjelm parallax—that it might be testable by precise models. Indeed, when we extrapolate our models to their parallax (the models calculated by Pourbaix et al. 1999 are too crude to be useful for comparisons here), we estimate that $Y_{ZAMS} = \sim 0.25$. This value is certainly on the low side of what one would expect for a slightly metal-rich star in our Galaxy and suggests to us that the Pourbaix parallax may be too low. We also note that the models that Pourbaix et al. constructed for α Cen A and B, based on their parallax determination, are too widely separated in age to be realistic models of α Cen A and B.

It is our opinion that *p*-mode observations will aid considerably our ability to test stellar structure and stellar evolution theory. Using α Cen AB as an example, we have outlined specific methodologies that use the *p*-mode large and small frequency spacings to help constrain the radius and convective core mass, respectively, of α Cen A. And we discuss the possibility of using the irregular frequency spacings between adjacent modes at low frequencies, which is

TABLE 6

α CEN B (MODEL B) $P-$MODE DATA

l	n	n_p	n_g	ν_{ad}	$\nu_{R:nonad}$	$\nu_{I:nonad}$	$\Delta\nu$	$\delta\nu$
0.....	2	2	0	642.2	642.2	0.00		
0.....	4	3	0	827.5	827.5	0.00		18.60
0.....	5	4	0	1009.9	1009.9	0.00	182.4	18.01
0.....	6	5	0	1191.3	1191.3	0.00	181.4	16.91
0.....	7	6	0	1372.5	1372.5	0.00	181.2	16.90
0.....	8	7	0	1550.7	1550.7	0.00	178.2	16.59
0.....	9	8	0	1727.8	1727.8	0.00	177.1	15.75
0.....	10	9	0	1902.2	1902.2	0.00	174.4	15.18
0.....	11	10	0	2072.5	2072.5	0.01	170.3	14.32
0.....	12	11	0	2240.8	2240.8	0.01	168.4	13.49
0.....	13	12	0	2408.2	2408.1	0.03	167.3	13.03
0.....	14	13	0	2575.0	2575.0	0.05	166.8	12.45
0.....	15	14	0	2742.0	2742.0	0.09	167.0	11.79
0.....	16	15	0	2907.7	2907.5	0.17	165.6	11.28
0.....	17	16	0	3071.8	3071.5	0.29	164.0	10.71
1.....	2	2	0	539.5	539.5	0.00		
1.....	3	3	0	726.3	726.3	0.00	186.8	42.04
1.....	4	4	0	910.2	910.2	0.00	183.8	34.56
1.....	5	5	0	1094.3	1094.3	0.00	184.2	32.67
1.....	6	6	0	1274.5	1274.5	0.00	180.2	30.82
1.....	7	7	0	1454.5	1454.5	0.00	180.0	28.82
1.....	8	8	0	1633.3	1633.3	0.00	178.9	28.08
1.....	9	9	0	1808.9	1808.9	0.00	175.6	26.63
1.....	10	10	0	1982.2	1982.2	0.00	173.2	25.12
1.....	11	11	0	2152.0	2152.0	0.01	169.9	24.23
1.....	12	12	0	2319.5	2319.5	0.02	167.5	23.16
1.....	13	13	0	2487.2	2487.2	0.04	167.7	22.29
1.....	14	14	0	2654.7	2654.6	0.07	167.5	21.66
1.....	15	15	0	2821.0	2820.9	0.13	166.2	20.64
1.....	16	16	0	2986.3	2986.1	0.22	165.3	19.69
2.....	2	2	0	618.9	618.9	0.00		
2.....	3	3	0	808.9	808.9	0.00	190.0	
2.....	4	4	0	991.9	991.9	0.00	183.0	
2.....	5	5	0	1174.4	1174.4	0.00	182.5	
2.....	6	6	0	1355.6	1355.6	0.00	181.2	
2.....	7	7	0	1534.1	1534.1	0.00	178.5	
2.....	8	8	0	1712.1	1712.1	0.00	178.0	
2.....	9	9	0	1887.0	1887.0	0.00	175.0	
2.....	10	10	0	2058.2	2058.2	0.00	171.1	
2.....	11	11	0	2227.4	2227.4	0.01	169.2	
2.....	12	12	0	2395.1	2395.1	0.02	167.8	
2.....	13	13	0	2562.6	2562.5	0.05	167.4	
2.....	14	14	0	2730.2	2730.2	0.09	167.6	
2.....	15	15	0	2896.4	2896.3	0.16	166.1	
2.....	16	16	0	3061.0	3060.8	0.28	164.6	
3.....	2	2	0	684.3	684.3	0.00		
3.....	3	3	0	875.6	875.6	0.00	191.3	
3.....	4	4	0	1061.6	1061.6	0.00	186.0	
3.....	5	5	0	1243.6	1243.6	0.00	182.0	
3.....	6	6	0	1425.7	1425.7	0.00	182.0	
3.....	7	7	0	1605.2	1605.2	0.00	179.6	
3.....	8	8	0	1782.3	1782.3	0.00	177.0	
3.....	9	9	0	1957.0	1957.0	0.00	174.7	
3.....	10	10	0	2127.8	2127.8	0.01	170.8	
3.....	11	11	0	2296.4	2296.4	0.02	168.6	
3.....	12	12	0	2464.9	2464.9	0.03	168.5	
3.....	13	13	0	2633.0	2633.0	0.06	168.1	
3.....	14	14	0	2800.3	2800.2	0.12	167.3	
3.....	15	15	0	2966.6	2966.5	0.21	166.2	

associated with mode bumping, to constrain the core structure and the age of the system. We also note that the mode-bumped frequencies could be extremely useful in establishing the l- and n-values of the observed p-modes.

We find that the small spacing is sensitive to both the composition and age and therefore cannot be directly used to infer the age of any individual star. But we point out that because α Cen A and B have the same age and ZAMS

composition, the small spacing may yet be useful as an age indicator. Here one would adjust the composition of the models of α Cen A and B until the small spacings of the models predict the same age for α Cen A as for α Cen B. When the composition is off, one would expect the ages predicted by the small spacings of α Cen A and B to be different. After some iteration one would end up with both an age and composition determination.

From our reference models (A and B in Tables 3 and 4, respectively) we estimate the large spacing $\langle \Delta\nu \rangle_A = 101 \pm 3$ μHz for α Cen A, and $\langle \Delta\nu \rangle_B = 173 \pm 6$ μHz for α Cen B.

The authors would like to thank Y.-C. Kim for initiating this project several years ago. The authors would also like to thank W. F. van Altena and his astrometry group for providing help in assessing the parallaxes. This work was supported in part by an NSERC grant to D.B.G.

REFERENCES

Aizenman, M., Smeyers, P., & Weigert, A. 1977, A&A, 58, 41
Alexander, D. R., & Ferguson, J. W. 1994, ApJ, 437, 879
Baglin, A., & Auvergne, M. 1997, in IAU Symp. 181, Sounding Solar and Stellar Interiors, ed. J. Provost & F.-X. Schmider (New York: Springer), 345
Böhm-Vitense, E. 1958, Z. Astrophys., 46, 108
Brown, T. M., et al. 1991, ApJ, 368, 599
Buzasi, D., Catanzarite, J., Laher, R., Conrow, T., & Kreidl, T. 2000, ApJ, submitted
Canuto, V. M., & Mazzitelli, I. 1991, ApJ, 370, 295
———. 1992, ApJ, 389, 724
Chan, K-L., & Sofia, S. 1987, Science, 235, 465
———. 1989, ApJ, 336, 1022
Chmielewski, Y., Friel, E., Cayrel de Strobel, G., & Bentolila, C. 1992, A&A, 263, 219
Demarque, P., Guenther, D. B., & Kim, Y.-C. 1999, ApJ, 517, 510
Demarque, P., Guenther, D. B., & van Altena, W. F. 1986, ApJ, 300, 773
Dravins, D., & Nordlund, Å 1990, A&A, 228, 203
Edmonds, P., Cram, L., Demarque, P., Guenther, D. B., & Pinsonneault, M. H. 1992, ApJ, 394, 313
Fernandes, J., & Neuforge, C. 1995, A&A, 295, 678
Flannery, B. P., & Ayres, T. R. 1978, ApJ, 221, 175
Fossat, E., Grec, G., Gelly, B., & Decanini, Y. 1984, CR Acad. Sci. Paris, Sér. 2, 229, 17
Green, E. M., Demarque, P., & King, C. R. 1987, The Revised Yale Isochrones and Luminosity Functions (New Haven: Yale Univ. Press)
Grevesse, N., Noels, A., & Sauval, A. J. 1996, in ASP Conf. Ser. 99, Cosmic Abundances, ed. S. S. Holt & G. Sonneborn (San Francisco: ASP), 117
Guenther, D. B. 1989, ApJ, 339, 1156
———. 1991, ApJ, 375, 352
———. 1994, ApJ, 422, 400
———. 1998, in Proc. SOHO 6/GONG 98 Workshop, Structure and Dynamics of the Interior of the Sun and Sun-like Stars, ed. S. Korzennik & A. Wilson (ESA SP-418), 375
Guenther, D. B., & Demarque, P. 1997, 484, 937
Guenther, D. B., Demarque, P., Buzasi, D., Catanzarite, J., Laher, R., Conrow, T., & Kreidl, T. 2000, ApJ, 530, L45
Guenther, D. B., Demarque, P., Kim, Y.-C., & Pinsonneault, M. H. 1992, ApJ, 387, 372
Guzik, J, A. 1998, in Proc. of the SOHO 6/GONG 98 Workshop, "Structure and Dynamics of the Interior of the Sun and Sun-like Stars," ed. S. Korzennik & A. Wilson (ESA SP-418), 417
Heintz, W. D. 1982, Observatory, 102, 42
Iglesias, C. A., & Rogers, F. J. 1996, ApJ, 464, 943
Kamper, K. W., & Wesselink, A. J. 1978, AJ, 86, 141
Kim, Y.-C. 1993, Ph.D. thesis, Yale Univ.
Kim, Y.-C., Fox, P. A., Demarque, P., & Sofia, S. 1996a, ApJ, 461, 449
Kim, Y.-C., Fox, P. A., Demarque, P., & Sofia, S. 1996b, in Proc. 32nd Liège Colloquium, ed. A. Noels, D. Fraipont-Caro, M. Gabriel, N. Grevesse, & P. Demarque (Liège: University of Liège), 195
Kim, Y.-C., Fox, P. A., Sofia, S., & Demarque, P. 1995, ApJ, 442, 422
Krishna Swamy, K. S. 1966, ApJ, 145, 174
Lydon, T. J., Fox, P. A., & Sofia, S. 1992, ApJ, 397, 701
———. 1993, ApJ, 413, 390
Noels, A., Grevesse, N., Magain, P., Neuforge, C., Baglin, A., & Lebreton, Y. 1991, A&A, 247, 91
Neuforge-Verheecke, C., & Magain, P. 1997, A&A, 328, 261
Nordlund, Å., & Stein, R. F. 1996, Proc. 32nd Liège Colloquium, ed. A. Noels, D. Fraipont-Caro, M. Gabriel, N. Grevesse, & P. Demarque (Liège: University of Liège), 75
Pourbaix, D., Neuforge-Verheecke, C., & Noels, A. 1999, A&A, 344, 172
Rogers, F. J., & Iglesias, C. A. 1996, Science, 263, 50
Rogers, F. J., Swenson, F. J., & Iglesias, C. A. 1996, ApJ, 456, 902
Schwarzschild, M. 1958, Structure and Evolution of the Stars (Princeton: Princeton Univ. Press)
Söderhjelm, S. 1999, A&A, 341, 121
Stein, R., & Nordlund, Å. 1989, ApJ, 342, L95
Ulrich, R. K. 1986, ApJ, 306, L37
Vitense, E. 1953, Z. Astrophys., 32, 135